Experimental methodology for the accurate stochastic calibration of catalytic recombination affecting reusable spacecraft thermal protection systems

Anabel del Val, Diana Luís, Olivier Chazot

Experimental methodology for the accurate stochastic calibration of catalytic recombination affecting reusable spacecraft thermal protection systems

Anabel del Val[a,b,*], Diana Luís[a], Olivier Chazot[a]

[a] *von Karman Institute for Fluid Dynamics, Chaussée de Waterloo 72, 1640 Rhode-St-Genèse, Belgium*
[b] *Platon Team, Inria/Centre de Mathématiques Appliquées, École Polytechnique, IPP, Route de Saclay, 91128 Palaiseau Cedex, France*

Abstract

This work focuses on the development of a dedicated experimental methodology that allows for a better stochastic characterization of catalytic recombination parameters for reusable ceramic matrix composite materials when dealing with uncertain measurements and model parameters. As one of the critical factors affecting the performance of such materials, the contribution to the heat flux of the exothermic recombination reactions at the vehicle surface must be carefully assessed. In this work, we first use synthetic data to test whether or not the proposed experimental methodology brings any advantages in terms of uncertainty reduction on the sought out parameters compared to more traditional experimental approaches in the literature. The evaluation is done through the use of a Bayesian framework developed in a previous work with the advantage of being able to fully and objectively characterize the uncertainty on the calibrated parameters. The synthetic dataset is adapted for testing ceramic matrix composites by carefully choosing adequate auxiliary materials whose heat flux measurements have the capability of reducing the resulting uncertainty on the catalytic parameter of the thermal protection material itself when tested under the same flow conditions. We then propose a comprehensive set of real wind tunnel testing cases for which stochastic analyses are carried out. The physical model used for the estimations consists of a 1D boundary layer solver along the stagnation line in which the chemical production term included in the surface mass balance depends on the catalytic recombination efficiency. All catalytic parameters of the auxiliary and thermal protection materials are calibrated jointly with the boundary conditions of the experiments. The testing methodology confirms to be a reliable experimental approach for characterizing these materials while reducing the uncertainty on the calibrated catalytic efficiencies by more than 50 %. An account of the posteriors summary statistics is provided to enrich the current state-of-the-art experimental databases.

Keywords: Thermal Protection System, Catalysis, Bayesian Inference, Uncertainty Quantification

1. Introduction

Traveling around and beyond our planet requires large amounts of energy, reaching velocities of the order of 7-11 km/s. All this amount of kinetic and potential energy is dissipated when a space vehicle enters dense planetary atmospheres. The bulk of this energy is exchanged during the entry phase by converting the kinetic energy of the vehicle into thermal energy in the surrounding atmosphere through the formation of a strong bow shock ahead of the vehicle. In general, a large fraction of the energy dissipated to the atmosphere is carried away from the vehicle through convection and radiation, leaving a small percentage to be absorbed back into the vehicle as thermal energy. A Thermal Protection System (TPS) is used to mitigate this heat load and ensure that the temperature limits of critical components on board are not exceeded during the entry phase. Prediction of the heating rate which is experienced by the TPS remains challenging, leading to very large safety margins for the vehicle design. Failing to correctly predict the heat loads and associated response of the TPS material during the design phase can lead to catastrophic

*Corresponding author: von Karman Institute for Fluid Dynamics, Chaussée de Waterloo 72, 1640 Rhode-St-Genèse, Belgium. *Email address:* ana.isabel.delvalbenitez@vki.ac.be (A. del Val)

mission failure. To address this problem, experimental facilities capable of generating high speed and plasma flows are developed to study different aspects of atmospheric entry flows [1], together with physico-chemical models used to describe the state of the flow at a given time and conditions [2].

Reusable heat shields are used for vehicles with moderate Earth entry velocities. They dissipate heat by re-radiating the energy back into the flow, and are designed to withstand multiple uses without need for replacement or substantial repair [3]. They are typically constructed from carbon or silicon carbide materials which have high emissivities at high temperatures to promote re-radiation. The interaction between the dissociated gas and the protection system is governed by the material behavior which acts as a catalyst for exothermic recombination reactions of the atomic species in the surrounding gas mixture [4].

Catalytic recombination is very ubiquitous in ground testing where typical TPS materials as well as other standard testing probes have catalytic properties that must be quantified to understand the experimental data. In the particular case of this work, the state-of-the-art experimental testing of such catalytic thermal protection materials at the von Karman Institute consists on using two different probes holding two different materials: a designated auxiliary material and the TPS material in question [5]. Both materials are tested under the same flow conditions at a time and the heat fluxes to their surfaces are recorded. The rebuilding of such parameters is heavily based on the choice of auxiliary material, whose catalytic properties are considered well-known. The reasoning behind this is that the catalytic behavior of the TPS material can be determined by performing a two-step rebuilding. The wall conditions for the auxiliary material are considered well-known so the outer edge conditions can be perfectly rebuilt through the inverse use of a fluid dynamic model in order to match the measured heat flux on the auxiliary probe. As both materials are tested under the same outer edge conditions (same run of the plasma wind tunnel), the wall conditions for the protection material under study can be rebuilt from the knowledge of the outer edge conditions by using the proposed fluid dynamic model in the same inverse fashion to recuperate the measured heat flux to the TPS probe. Viladegut and Chazot [6] took this exercise further by characterizing the catalytic properties of the most common auxiliary material used in the experiments, copper, given that very different values are recalled in the relevant literature. Through their work, Viladegut and Chazot developed a 3-probes testing methodology aimed at better characterizing copper catalytic properties for future uses on experiments with TPS materials.

This type of rebuilding techniques spans beyond the facility at the von Karman Institute, affecting the results reported in the broader literature for catalysis determination [7–11]. The fact that the reconstruction work is still considered a well-defined process with known characteristics, makes the following question not worth asking: how should we perform experiments in order to get the most information regarding catalytic coefficients under uncertain observations and model parameters? The identification of uncertainty sources and how to deal with them unveils a new set of issues, namely, how well we can learn the catalytic parameters we are after and how to improve such estimation by acting on our experimental methodologies. The previously trivial question now acquires central relevance if we want to move forward in the quest for predictive models. The more informative our experiments get, the more useful are the data to increase the confidence in our models or, conversely, invalidate them. This brings up another important aspect of catalysis determination: the production of high-quality wind tunnel data given the ubiquitous nature of this phenomenon among ground testing probes. Special care should be devoted to the fact that as the number of model parameters that need definition increases with the model complexity [12], the experimental data obtained for such high temperature, reacting flows are too often pretty scarce for proper validation studies. Assuming values for model parameters becomes a common exercise when simulating experimental conditions against which to compare our models, potentially biasing the obtained results with partial understanding of the problem. Producing specifically tailored calibration data to inform some of such parameters is becoming increasingly relevant in validation tasks [13]. Tackling all these issues is important for ensuring the reliability of model predictions under various types of uncertainties, as well as producing data from which validation of models is possible.

In a previous work, del Val et al. [14] presented a Bayesian framework able to exploit more thoroughly plasma wind tunnel data for catalysis determination. Results showed a posterior support that is reduced in half compared to the prior support. The marginal posterior distributions also showed well-defined peaks. It was concluded that catalytic efficiencies can be learned from heat flux and wall temperature measurements, although the uncertainty levels on the posterior distributions were still large for a precise characterization. As part of that same work, del Val et al. studied the influence of different characteristics of the experimental set-up which are freely chosen by the experimentalists a priori, such as the type of auxiliary material as well as the number of auxiliary materials tested jointly with the TPS material itself. The results motivated the current work for which the objectives are twofold: first, to show how

proposing experiments for catalysis testing must change when introducing uncertain hypotheses and observations. Second, to provide a first database of catalytic parameters for Ceramic Matrix Composite (CMC) materials and their corresponding testing boundary conditions with associated probability distributions and confidence levels so that future validation is possible. The first objective is tackled by proposing a synthetic dataset to test whether or not the main characteristics of the envisaged 3-probes experimental approach bring any advantages in terms of uncertainty reduction on the sought out parameters compared to the more traditional experimental approaches in the literature. Real wind tunnel tests are then carried out for a set of seven test cases under different static pressures and heat fluxes to study and discuss their influence on the results. Finally, the summary statistics of the results are computed constituting the first CMC catalysis database with associated accurate characterization of their uncertainty.

The article is organized as follows. Section 2 describes the facility and experimental set-up proposed. In Section 3, the model-based simulations and Bayesian framework are presented in detail. Section 4 shows the testing conditions and discusses the results obtained from the Bayesian analysis. Section 5 summarizes the outcomes of the analyses and discusses the possible perspectives of the presented approach.

2. Experimental facility and proposed set-up

As we have seen from the introduction to this article, new questions arise in how to devise experiments once we accept and deal with uncertainty sources. As it has been highlighted, the state-of-the-art catalysis reconstruction assumes the fact that we are able to perfectly characterize the environment under which a TPS material is being tested, namely, all the fluid variables at the boundary layer inlet. In accepting this premise, we can then trace back the heat flux on the TPS sample to the catalytic activity under a prescribed thermal and chemical state of the flow if the surface temperature is measured along. When acknowledging the facts that we can only get noisy observations from the tests and that the assumptions about the edge conditions/auxiliary material are quite uncertain, we need to propose experiments that better inform the sought out catalytic parameters in the presence of such uncertainties.

In this section, we introduce the experimental set-up installed in the Plasmatron facility, together with a description of the facility and intrusive/non-intrusive measurement techniques.

2.1. Plasmatron facility description

The Plasmatron at the von Karman Institute (VKI) is an Inductively-Coupled Plasma (ICP) wind tunnel [15] that offers an ideal environment for catalytic studies due to the production of plasma jets of very high chemical purity [16]. Bottin [17] and Bottin et al. [15] have extensively studied this facility and a detailed description may be found in their works. Its basic concept consists of a quartz tube surrounded by a coil which is connected to a generator that provides high voltage (1.2 MW) and high frequency (400 kHz) current. This induces an electromagnetic (EM) field inside the tube, that forces residual charged particles in the flow to form eddy currents which heat up the gas by Joule effect. The gas is injected through a ring-shaped inlet at the outer edge of the torch. Due to the induced EM field, the gas ionizes into plasma discharge which exits as a subsonic flow into a low pressure test chamber that hosts material probes. Argon is employed as starting gas, facilitating the initial electric discharge due to the longer lifetime of the free electrons at low pressure compared to the air plasma case. Complementary systems are responsible for the gas circulation, probes, cooling, and diagnostics. Selected testing materials are mounted onto holders which are remotely activated to be injected and retracted from the plasma jet. Suitable windows provide the necessary optical access to the testing chamber for the flow and sample diagnostics: the lateral windows (on both sides of the wind tunnel) allow perpendicular side views of the plasma jet and probes, and the the torch-side windows allow a frontal oblique view of the material surfaces.

A picture of the set-up is included in Figure 1. In the picture, we can clearly see the exit of the torch from which the generated plasma flow is discharged into the testing chamber where the test samples are held. The VKI Plasmatron can host different measurement techniques, such as intrusive probes for heat flux and dynamic pressure measurements, as well as non-intrusive optical techniques whose accesses to the testing chamber are highlighted in the picture.

2.2. Proposed set-up and methods

As the edge quantities that characterize the environment under which a TPS material is being tested cannot be measured directly with confidence, we are drawn to propose indirect ways to characterize such flow conditions.

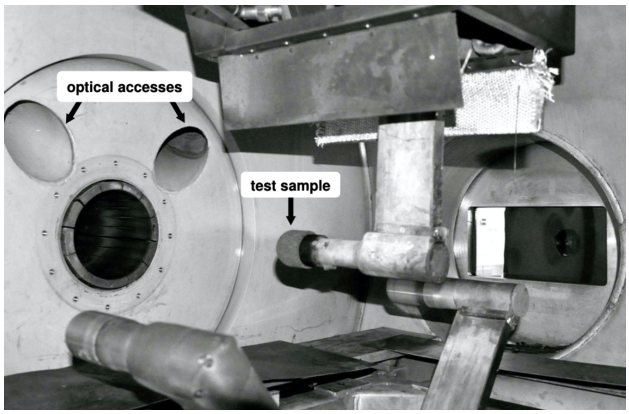

Figure 1: Experimental set-up in the Plasmatron facility.

Most of the proposed experimental set-up, as already reflected in the relevant literature [5, 18–20], is devoted to the characterization of such conditions when the measurements and knowledge of our system are not perfect. The chosen set-up rests on two different auxiliary materials following the experimental design of Viladegut and Chazot [6]. We refer to this general set-up as 3-probes testing methodology given that it uses two different auxiliary materials along with the TPS sample in question. The novelty introduced in this work is the choice of the auxiliary materials that accompany the testing of the CMC samples as well as the fact that the 3-probes testing methodology has not been used before for better characterization of TPS materials. Apart from the novelties in the set-up itself, there is also novelty in the way we arrive at the proposed set-up by strictly performing stochastic analyses on synthetic data. In other words, by finding constraints on the model parameters sought out through a devised experimental set-up.

Coupling the 3-probes testing methodology with the analyses shown by del Val et al. [14] on the choice of auxiliary materials, we are drawn to propose a set-up in which the CMC TPS material surface catalysis can be framed between a lower and upper catalysis levels ideally found in the auxiliary materials of choice. In this case, the upper catalytic material is an obvious choice, being copper the most studied material for this kind of testing [21–29]. The lower catalytic material is more challenging due to the nature of TPS materials, designed to purposefully be of low surface catalytic activity. Furthermore, evidence of oxidation of the SiC coating of CMC materials can also impact the catalytic activity on such TPS surfaces [16]. Nevertheless, we find a good option in quartz from the experimental results of Viladegut and Chazot [6] when compared to the tests of Panerai and Chazot [16] for CMC materials under the same flow conditions given different wall temperatures. This choice is first tested on synthetic data to corroborate the good choice before attempting the real experiments. The major hurdle in the way of the proposed set-up is that for achieving the full potential of the 3-probes methodology, the TPS material and quartz should have catalytic responses that differ significantly. If the CMC material responds similarly to quartz, adding quartz to the tests would not bring any new information. The results with the proposed methodology would effectively be as 2-probes testing cases in terms of uncertainties on the CMC catalytic parameters, giving out similar results as the case study of [14]. Even though the oxidation of the SiC coating on the TPS material surface causes SiO_2 (quartz) to form, the differences in wall temperatures can make the TPS and quartz catalytic responses differ enough to achieve good characterizations. Furthermore, microscopic considerations on the oxidized TPS layer could also prevent both catalytic responses from being very similar.

Fig. 2 presents the experimental set-up proposed for this study. Copper, TPS and quartz samples are mounted on probe holders and are sequentially exposed to the same plasma flow. In these experiments, "standard" ESA geometry probes (also known as Euromodel) for typical non-equilibrium boundary layers, with a radius of 25 mm, are used.

To calibrate the plasma flow conditions, we use two water-cooled 14 mm (sensing area) copper and quartz calorimeters. They measure the cold wall heat flux at the stagnation point ($T_w^{Cu} \approx 350$K and $T_w^{Qz} \approx 750$K, respectively). These heat fluxes are determined by the water mass flow ($\dot{m}$), which is controlled by a calibrated rotameter, and the temperature difference ($T^i_{out} - T^i_{in}$) in the cooling water supply. Thus, the heat flux for the cold wall probes (q^i_w) is given by the expression

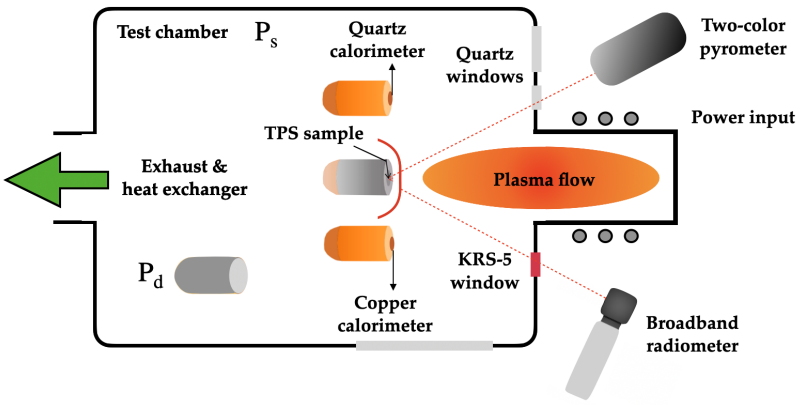

Figure 2: Schematic of the experimental set-up (seen from top, not to scale) with pyrometer and radiometer optical paths in front of the TPS material sample.

$$q_w^i = \frac{\dot{m} c_p (T_{out}^i - T_{in}^i)}{A} \quad \forall i \in \text{Cu, Qz}, \tag{1}$$

where c_p is the water specific heat and A the area of the surface of the probe. The cold wall heat flux probes are injected into the plasma flow once the air mass flow and chamber pressure are stabilized. The dynamic pressure (P_d) is measured using a Valydine differential pressure transducer and the static pressure (P_s) in the Plasmatron chamber is measured by an absolute pressure transducer (Memberanovac DM 12, Leybold Vacuum, OC Oerlikon Corporation AG). As the Plasmatron only has three probe holders, the dynamic pressure is recorded during a different test case, where the copper heat flux and pressures of the first experimental run are duplicated.

To analyse the surface temperature and emissivity of the TPS material, a two-colour pyrometer and an infrared radiometer are used. As previously mentioned, cold wall heat flux and pressure probes are used for jet calibration. The optical instruments (pyrometer and radiometer) are calibrated with the aid of a black-body (BB) source (LANDCAL R1500T, LAND Instruments International), which provides a reference temperature spot with an emissivity value close to 1. The calibration procedure used can be found in Helber [19]. A two-colour Raytek Marathon Series MR1S-C infrared pyrometer with an operating range between 1000 and 3000 °C is used. Optical access to the testing chamber is offered through a 1 cm thick quartz window, placed at $\sim$ 1 m distance to the probe, with an orientation of 35° with respect to the stagnation line. To record the surface radiance, a broadband infrared radiometer (KT19, HEITRON-ICS Infrarot Messtechnik GmbH) is used. This instrument is located at 47° angle relative to the surface normal in front of a 1.8 cm thick KRS-5 window, which offers $\sim$ 70 % optical transparency [16] in the whole infrared range of the instrument (0.39 – 0.6μm). Its temperature range is between 0 and 3000° C and the acquisition frequency is set to 1 Hz. The output provided is the integrated thermal radiation over the spectral range, converted into equivalent temperature through an adjustable emissivity value which, in the context of the Plasmatron facility, is set to one. As the range between 0.39 – 0.6μm contains the highest percentage of thermal radiation at the operation temperatures of the Plasmatron [16], the actual radiance and emissivity can be computed with the Stefann-Boltzmann law as a fast approximation. Being T_w^{pyro} the real surface temperature acquired by the pyrometer and T_w^{radio} the equivalent temperature measured by the radiometer, the total emissivity can be determined as

$$\varepsilon = \frac{(T_w^{radio})^4}{(T_w^{pyro})^4}. \tag{2}$$

Emissivity being derived from the measurements of the pyrometer and radiometer, we can now estimate the actual heat flux to the TPS sample by assuming radiative equilibrium as

$$q_w^{TPS} = \sigma \varepsilon \left(T_w^{pyro}\right)^4, \tag{3}$$

where σ is the Stefan-Boltzmann constant and T_w^{pyro} is the actual TPS material temperature measured with the pyrometer and referred to as T_w^{TPS} in the remaining of this work.

All the measured quantities here described present inherent uncertainties. These uncertainties are due to the limited precision of the measuring devices as well as statistical deviations due to the finite number of possible repetitions of such measurements to derive a proper statistical distribution. In the case of the measurements described previously in this section, the measurement uncertainty model is taken as independent unbiased Gaussian distributions. Mean values represent the most likely outcome of the measurements while standard deviations reflect the precision and statistical fluctuations. It is important to take into account the fact that the measured quantities are not the raw experimental measurements but calibrated and post-processed quantities. A forward propagation of uncertainties is needed to estimate properly the uncertainty levels (standard deviations of the Gaussian distributions) of the different post-processed quantities. In the limit case where properties of the experimental apparatus (specific heat of water c_p and area A used in Eq. (1), for example) are not perfectly known, preliminary measurements may be needed to calibrate the unknowns of the measurement chain through a Bayesian inference framework. The calibrated coefficients of the system together with the raw experimental data should then be forwardly propagated to obtain accurate uncertainty estimates on the measured quantities.

The focus of this contribution is not to properly define the experimental uncertainties involved in the set-up measurement chains. That would entail the development of a whole set of frameworks for each measurement technique, involving calibration data. The objective of the article is centered around the possible improvement of the characterization of catalytic efficiencies for TPS materials through experimental design alone, given experimental uncertainties consistent with the current state-of-the-art Plasmatron testing for comparison. In this case, the uncertainty estimates considered here are computed in agreement with the methodologies followed in the available literature for experiments in the Plasmatron facility [5, 19]. The distributions associated to the static pressure P_s, dynamic pressure P_d, wall heat fluxes q_w^{Cu}, q_w^{Qz} and q_w^{TPS}, and surface temperatures T_w^{Cu}, T_w^{Qz} and T_w^{TPS} are given in Sec. 4.

2.3. On the differential pressure transducer measurements

The experiments are performed with three sample probes (copper, TPS and quartz) which is the maximum available probes to test in a single run in the Plasmatron facility. Apart from the heat fluxes to the three materials of choice, we need a probe to mount the pressure transducer which measures the dynamic pressure P_d. For each defined testing case, a second experimental run is performed for the recording of the dynamic pressure. Together with the pressure transducer probe, the water-cooled copper calorimeter is also tested to give a reference for the testing conditions by looking at the resulting copper heat flux measurement.

A correlation is established between heat flux and Pitot measurements [20], and linear regressions for given static pressure and mass flow conditions are obtained with the copper heat fluxes and dynamic pressures measured in the calibration run. The actual value of the dynamic pressure in the first run is computed through the linear regressions for the copper heat flux measured in the first run.

More details can be found in Appendix A.

3. Model-based simulations and Bayesian inference methodology

The plasma flow produced in the experiments and its interactions with the different materials are simulated using a reacting boundary layer solver. The pieces missing in the modeling are to be recovered from the experimental data to a certain degree of precision allowed by the design of the experimental set-up, the measurement techniques and our knowledge of the flow state and assumptions behind it. In this section, we present the model and theoretical assumptions and briefly recall the Bayesian inference methodology.

3.1. Reacting boundary layer model

In this work, we are primarily interested in the simulation of catalytic interactions between the hot plasma flow and the exposed material surface. As these interactions happen in a thin layer around the face of the material, we can reduce the computational domain to just the boundary layer which contains the physics of the phenomena we want to study. Focusing on the boundary layer instead of the full flow domain offers a great deal of simplification over the full set of the Navier-Stokes equations, both in terms of mathematical and numerical complexity. Moreover, we only

need to focus our attention on simulating the stagnation line given that the relevant experimental information available generally refers to the probes' stagnation point quantities. In this work, we simulate the chemically reacting boundary layer in the vicinity of the probe stagnation point [30] using the 1D boundary layer solver developed by Barbante [31], given its efficiency and physical completeness in simulating the relevant features of the experiments.

To solve the system, we need closure models for the thermodynamic and transport properties as well as the chemical production terms of the different species. Transport fluxes are derived from kinetic theory using the Chapman-Enskog method for the solution of the Boltzmann equation [32, 33]. Diffusion fluxes are computed through the generalized Stefan-Maxwell equations, an approach which by derivation is exactly equivalent to a description based on the multicomponent diffusion matrix [34–36], therefore providing equivalent solutions for the diffusion fluxes. For the homogeneous chemistry in the gas phase, the Law of Mass Action is used to compute production rates as proportional to the product of the reactant densities raised to their stoichiometric coefficients [37]. A 7-species air mixture and chemical rates from Dunn and Kang [38] in the form of modified Arrhenius laws are considered. The thermodynamic properties, such as the enthalpy, are derived from statistical mechanics [30, 39] for a reacting mixture of perfect gases, assuming thermal equilibrium and chemical non-equilibrium. Apart from the closure models, the parabolic nature of the Boundary Layer (BL) equations requires the imposition of two boundary conditions: the external flow conditions at the boundary layer edge, and the conditions at the material surface. A mass balance is imposed to account for the production and depletion of species as a consequence of their interactions with the material surface. Recombination reactions can be triggered depending on the catalytic activity of such material [40]. We impose a no slip condition at the wall for the momentum equation and impose a wall temperature for the energy flux. More details about the derivation, coordinate transformations and numerical implementation of the BL code are available in the work of Barbante [31]. In summary, the predictive quantity of the code is the wall heat flux which can be expressed through a relationship with the hydrodynamic parameters needed to close the flow equations

$$q_\mathrm{w} = q_\mathrm{w}\left(\gamma, T_\mathrm{w}, P_\delta, H_\delta, \delta, \left.\frac{\partial u}{\partial x}\right|_\delta, v_\delta \frac{\partial}{\partial y}\left(\frac{\partial u}{\partial x}\right)\Big|_\delta\right). \tag{4}$$

The free stream parameters are denoted with subscript δ which refers to the boundary layer thickness. The coordinates x and y denote the radial and axial directions along the stagnation line, respectively. The last two arguments are the velocity gradient at location δ, which controls the local chemistry by imposing the residence time of the flow around the stagnation point, and the axial velocity times the derivative of the velocity gradient at location δ, respectively. This last quantity is included in the formulation to account for the fact that the free stream flow is highly viscous, unlike in classical boundary layer formulations. To match the outer flow solution to the boundary layer solution, the last argument in Eq. (4) has to be imposed to account for the extrapolation to the wall of the external flow pressure gradient in the axial momentum equation [31].

If we did not have any more information about our experiments, we would have to assume that all boundary layer edge conditions are unknown and we would have to estimate them along the model parameters of interest. On closer inspection, the experimental boundary layer is generated by the VKI Plasmatron and its characteristics closely depend on the operating conditions selected for the experiments. Given this information, we can recuperate some boundary layer edge parameters that depend on the facility operating conditions and do not play such an important role in the inferences we want to undertake. This allows us to estimate these parameters and used them as given quantities for the inferences.

The subsonic VKI Plasmatron flowfield, composed by the torch and test chamber, is numerically simulated using an axisymmetric LTE magnetohydrodynamics solver which computes the solution of the Navier-Stokes equations coupled to the Maxwell's equations under certain assumptions (VKI ICP code [2, 41, 42]). Initially developed as a standalone tool, the VKI ICP code is nowadays integrated into the Computational Object-Oriented Library for Fluid Dynamics (COOLFluiD) [43]. The ICP simulation takes the inlet mass flow $\dot{m}$, the power transmitted to the plasma from the coils P_plasma, the chamber static pressure P_s and the probe geometry as inputs. The power transmitted to the plasma flow is a percentage of the total power injected to the coils P_el. This percentage is usually taken as 50% [44].

The governing equations rely on the MUTATION^{++} library [45] for the computation of the thermodynamic and transport properties of air with eleven species mixture: $\{\mathrm{O_2}, \mathrm{N_2}, \mathrm{O_2^+}, \mathrm{N_2^+}, \mathrm{O}, \mathrm{N}, \mathrm{O^+}, \mathrm{N^+}, \mathrm{NO}, \mathrm{NO^+}, \mathrm{e^-}\}$. From the VKI Plasmatron simulations we can obtain the local momentum characteristics at the edge of the boundary layer we are trying to reproduce. For this, we can compute Non-Dimensional Parameters (NDPs) that define the boundary layer

thickness δ, the velocity gradient $(\partial u/\partial x)\Big|_\delta$, and the axial gradient of the velocity gradient $(\partial\,(\partial u/\partial x)\,/\partial y)\Big|_\delta$ [44, 46]. The dynamic pressure, corrected for viscous effects $P_\mathrm{d}/K_\mathrm{H} = 1/2\rho_\delta v_\delta^2$ with K_H as Homman's correction factor [47], is used as a convenient proxy for the axial velocity v_δ in Eq. (4) given that it is a measured quantity [48]. As we are assuming a boundary layer edge in chemical equilibrium, the density ρ_δ in the dynamic pressure expression is defined by the enthalpy H_δ and pressure P_δ. The variability of the non-dimensional parameters with the operating conditions is small as shown by Panerai [5], therefore they can be considered known constants for each experiment [49]. Finally, for given VKI Plasmatron operating conditions, the predictions we are seeking to match the experimental data are now recast as

$$q_\mathrm{w} = q_\mathrm{w}\left(\gamma, T_\mathrm{w}, P_\delta, H_\delta, P_\mathrm{d}\right), \tag{5}$$

where P_δ is taken as the chamber static pressure P_s, and the momentum boundary layer edge conditions have been replaced by the dynamic pressure, given that the non-dimensional parameters are taken as constants. These parameters, together with the dynamic pressure P_d, define the boundary layer thickness, velocity and derivatives at the edge. Even though the number of input parameters is larger in Eq. 5, this formulation is more useful. In this case, we have replaced three unknown and not easily measurable quantities by a quantity that can be directly measured (P_d) and three parameters that do not depend on the local flow conditions. The latter can be taken as known constants for each condition for the purpose of our Bayesian formulation.

Only the measurements of the heat fluxes carry the information of the catalytic parameters γ in an implicit relation seen in Eq. 5, given that there is not a surface energy balance to be solved for the surface temperatures. All the other quantities are taken as inputs of the BL code while the heat fluxes are the outputs of the different simulations. This aspect, together with the fact that there is not a measured counterpart for the enthalpy H_δ, define the characteristics of the proposed Bayesian formulation of the inference problem in subsequent sections.

3.2. Bayesian inference methodology

The inference of model parameters uses the Bayes formula which can be generically formulated as

$$\mathcal{P}(\boldsymbol{q}|\mathcal{M}) = \frac{\mathcal{P}(\mathcal{M}|\boldsymbol{q})\,\mathcal{P}(\boldsymbol{q})}{\int_\Omega \mathcal{P}(\mathcal{M}|\boldsymbol{q})\,\mathcal{P}(\boldsymbol{q}) d\boldsymbol{q}}, \tag{6}$$

where $\boldsymbol{q}$ is the vector of parameters, having for components the parameters of the analysis, and $\mathcal{M}$ is the vector of the measured quantities. In the present Bayesian setting, $\boldsymbol{q}$ and $\mathcal{M}$ are real-valued random vectors. We denote $\mathcal{P}(\boldsymbol{q})$ the prior probability distribution of the parameters that expresses one's beliefs on possible values of $\boldsymbol{q}$ before the measurements are made available. $\mathcal{P}(\mathcal{M}|\boldsymbol{q})$ is the likelihood function, i.e., the probability of observing measurements $\mathcal{M}$ given $\boldsymbol{q}$. Typically, the likelihood compares the measurements with model predictions (functions of $\boldsymbol{q}$), and relies on a noise model to account for the measurement error; a model error contribution can also be included [50]. Specifically, the comparison can be made on the raw measurements or more generally on some derived quantities which is the case of our study. From the measurements $\mathcal{M}$, we can update the prior distribution $\mathcal{P}(\boldsymbol{q})$ to the posterior probability distribution $\mathcal{P}(\boldsymbol{q}|\mathcal{M})$ by using the experimental data $\mathcal{M}$.

The posterior distribution in Eq. 6 is usually not known in a closed form due to the complexity of the mapping $\boldsymbol{q} \rightarrow M(\boldsymbol{q})$ where $M(\boldsymbol{q})$ is the vector of model predictions using the forward model. The error models can also complicate calculations. Therefore, sampling strategies, such as Markov Chain Monte Carlo (MCMC) methods [51], are needed to estimate the statistics of the posterior distribution of $\boldsymbol{q}$ (e.g., mean, moments, median, and mode). In this work, we use the Adaptive Metropolis (AM) algorithm [52], an extension of the Random-Walk Metropolis (RWM) algorithm, which adapts the proposal covariance matrix using previously sampled points.

The main drawback of the MCMC approach is that it generally requires a large number of evaluations of the forward model $M(\boldsymbol{q})$. In our case, this means solving a system of coupled PDEs in one dimension with auxiliary problems for the closure terms at least thousands of times. As a result, the approach would be computationally intractable. Instead, we derive a surrogate model $\hat{M}(\boldsymbol{q})$, with low evaluation cost and good accuracy, that can be used in place of the original model $M(\boldsymbol{q})$ in the likelihood, as proposed in other works such as [53]. If the surrogate model can be constructed at a reasonable computational cost, the sampling of the posterior distribution can be orders of magnitude faster and cheaper than the direct sampling using the full forward problem.

Lastly, the integral under the denominator in Eq. 6 extends to the space of $\boldsymbol{q}$, denoted here with the Greek letter Ω. In practical terms, this integral is called the evidence and it is a single number. It usually does not mean anything by itself, but becomes useful when we compare one evidence with another evidence. Formally, the evidence is a likelihood function. Specifically, it is the completely marginalized likelihood function. It is therefore sometimes denoted $\mathcal{P}(\mathcal{M})$ with no $\boldsymbol{q}$ dependence. It can be thought as the probability that the measurements are obtained under the considered model.

3.2.1. Prior distribution and likelihood function

The posterior distribution for our Quantities of Interest (QoI) can be cast into a ratio of probabilities

$$\mathcal{P}(\boldsymbol{\gamma}|\mathcal{M}) = \frac{\mathcal{P}(\mathcal{M}|\boldsymbol{\gamma})\,\mathcal{P}(\boldsymbol{\gamma})}{\mathcal{P}(\mathcal{M})}, \tag{7}$$

where the vector of parameters $\boldsymbol{q}$ is denoted as $\boldsymbol{\gamma} = (\gamma_{\mathrm{Qz}}, \gamma_{\mathrm{TPS}}, \gamma_{\mathrm{Cu}})$, the set of recombination parameters to be inferred, and $\mathcal{M} = (q_{\mathrm{w}}^{\mathrm{Qz,meas}}, q_{\mathrm{w}}^{\mathrm{Cu,meas}}, q_{\mathrm{w}}^{\mathrm{TPS,meas}}, T_{\mathrm{w}}^{\mathrm{Qz,meas}}, T_{\mathrm{w}}^{\mathrm{Cu,meas}}, T_{\mathrm{w}}^{\mathrm{TPS,meas}}, {P_{\mathrm{s}}}^{\mathrm{meas}}, {P_{\mathrm{d}}}^{\mathrm{meas}})$ is the set of available measurements. The prior probability distribution $\mathcal{P}(\boldsymbol{\gamma})$ can be expressed as the product of three independent priors prescribed for each model parameter $\mathcal{P}(\boldsymbol{\gamma}) = \mathcal{P}(\gamma_{\mathrm{Qz}})\,\mathcal{P}(\gamma_{\mathrm{TPS}})\,\mathcal{P}(\gamma_{\mathrm{Cu}})$. All prior probability distributions are taken as log-uniform within selected intervals, with constraints on the normalization factor (integral of the distribution is equal to one). This way, no assumptions are made about the catalytic behavior of the auxiliary materials compared to the TPS material under study given that we assume the same knowledge for all a priori. This choice of priors also ensures compliance with the maximum entropy principle [54]. The particular supports chosen are $\log_{10}(\gamma_{\mathrm{Qz}}),\ \log_{10}(\gamma_{\mathrm{TPS}}),\ \log_{10}(\gamma_{\mathrm{Cu}}) \sim \mathcal{U}(-4, 1)$. The motivation behind such priors can be found in del Val et al. [14].

As all materials should play the same role in the inference problem, a likelihood function accounting for the whole set of available measurements is proposed following the work of del Val et al. [14]. This likelihood function quantifies the amount of information carried by the measurements $\mathcal{M}$ to the QoIs $\boldsymbol{\gamma}$. As not all the different quantities needed to simulate a reacting boundary layer can be measured or known (such as the flow enthalpy at the inlet boundary), del Val et al. proposed an optimization procedure built on the construction of the likelihood function to determine their most likely values based on the available experimental data. This procedure avoids the need to introduce any a priori estimates on the nuisance quantities, namely, the boundary layer edge enthalpy, static and dynamic pressures, and wall temperatures, which would entail the use of very wide priors.

Assuming that the discrepancy between the measurements and predictions are only due to the measurements noise, we propose an error model that follows independent unbiased Gaussian distributions. Accordingly, the likelihood function takes the form

$$\begin{aligned}\mathcal{P}^{\mathrm{opt}}(\mathcal{M}|\boldsymbol{\gamma}) \propto \exp\left[-\frac{({P_{\mathrm{s}}}^{\mathrm{meas}} - {P_{\mathrm{s}}}^{\mathrm{opt}}(\boldsymbol{\gamma}))^2}{2\sigma_{P_{\mathrm{s}}}^2}\right] \exp\left[-\frac{({P_{\mathrm{d}}}^{\mathrm{meas}} - {P_{\mathrm{d}}}^{\mathrm{opt}}(\boldsymbol{\gamma}))^2}{2\sigma_{P_{\mathrm{d}}}^2}\right] \times \\ \times \prod_{i\in\ \mathrm{Qz,TPS,Cu}} \exp\left[-\frac{\left(q_{\mathrm{w}}^{i,\mathrm{meas}} - q_{\mathrm{w}}^{i,\mathrm{opt}}(\boldsymbol{\gamma})\right)^2}{2\sigma_{q_{\mathrm{w}}}^2} - \frac{\left(T_{\mathrm{w}}^{i,\mathrm{meas}} - T_{\mathrm{w}}^{i,\mathrm{opt}}(\boldsymbol{\gamma})\right)^2}{2\sigma_{T_{\mathrm{w}}}^2}\right],\end{aligned} \tag{8}$$

where ${P_{\mathrm{s}}}^{\mathrm{opt}}, {P_{\mathrm{d}}}^{\mathrm{opt}}, T_{\mathrm{w}}^{i,\mathrm{opt}}$ are the quantities that maximize the likelihood function, and $q_{\mathrm{w}}^{i,\mathrm{opt}}$ the resulting predictions of the heat fluxes for each of the three material samples when using the maximizers of Eq. (8) as inputs. These maximizer quantities are only function of $\boldsymbol{\gamma}$, obtaining as a result a likelihood that only depends on the QoIs. Finally, the term $\mathcal{P}(\mathcal{M})$ can be omitted given that in a MCMC setting we rely on the computation of ratios of the posterior for which the denominator is cancelled out.

The optimization algorithm for the computation of the likelihood function is the Nelder-Mead algorithm [55]. Applying an optimization method prevents us from using directly this approach to sample the posterior distribution due to high computational time. Each point of the sampling space is the result of an optimization procedure which takes hundreds of realizations of the numerical solver. To overcome this limitation, we build a surrogate model for the log-likelihood of the problem.

3.2.2. Surrogate modeling

The surrogate model is built by considering the log-likelihood as a function of $\log_{10}\boldsymbol{\gamma}$, the log-variables, which we consequently normalise and refer to as $\boldsymbol{\beta}$. In particular, we seek to construct a surrogate of the optimal likelihood $\mathcal{P}^{\text{opt}}(\mathcal{M}|\boldsymbol{\beta})$ with this parametrization. We decided to proceed with the log-likelihood instead of the likelihood as it ensures the positivity of the approximation and shows a smoother behavior. More precisely, we aim for a surrogate model of $Y(\boldsymbol{\beta})$ defined by

$$Y(\boldsymbol{\beta}) \doteq \log\left(\mathcal{P}^{\text{opt}}(\mathcal{M}|\boldsymbol{\beta})\right).$$

We choose Gaussian Processes (GP) for this task. Due to their statistical nature, GP provide both a prediction of the approximated function and a measure of the uncertainty (variance) in the prediction. To this end, we consider a three dimensional grid in the space of $\boldsymbol{\beta}$ and evaluate the corresponding values of the log-likelihood. In this work, we employ what it is known as model-free Design of Experiments (DoE) which does not rely on model evaluations as an active learning strategy would require [56]. Model-free DoEs are concerned with optimizing the exploration of the input space with a finite set of points. In this case, we build a uniform grid for the optimal log-likelihood approximation (Eq.(8)) and use a Latin Hypercube Sampling (LHS) algorithm, introduced by McKay et al. [57]. The LHS sampling algorithm presents the advantage of allowing us to survey the input space by devising a space filling strategy adapted to the inputs probability distributions. This strategy consists of dividing the range of each variable into n equally probable intervals in which sampling is performed at random in our case. The initial sparse LHS grid, upon which we build the first GP surrogate, spans the prior bounds of $\boldsymbol{\beta}$. The GP surrogate is used in place of the exact likelihood function to sample the posterior distribution by means of the MCMC algorithm chosen. In subsequent iterations of this procedure, the additional sampling domain becomes smaller, focusing only on the part of the domain where the MCMC algorithm is drawing samples from, refining the accuracy of the GP in that region. The stopping criteria is chosen when the variance of the GP in the refined region (from where we draw the posterior samples) reaches the threshold value of 1%. We choose the same kernel and GP characteristics as del Val et al. as they are particularly fitted for this task.

4. Results and discussion

In this section, we first perform a study of synthetic data. The study allows us to gauge the viability of the methodology in terms of well defined posteriors for the TPS catalytic parameters which is what we are looking for in defining these experiments.

Consequently, we apply the methodology previously discussed to real tests performed in the Plasmatron facility. A brief discussion on the testing conditions selected is followed by the analyses of the results.

4.1. Test cases based on synthetic data

As a proof of concept, the 3-probes testing methodology works well when the materials tested have a range of different catalytic responses to the incoming flow [14]. We could devise a synthetic case with the boundary layer solver where the catalytic parameters of copper, quartz and TPS get assigned values consistent with the literature. The corresponding synthetic observations such as heat fluxes and pressures can be corrupted by noise also consistent with the measuring devices. From these synthetic observations we could check if we could infer the catalytic parameters initially assigned and study the quality of the posterior distributions. The problem with this common approach in our case is that the catalytic parameter values consistent with the literature are already compromised based on a priori knowledge about the corresponding auxiliary materials. Our synthetic case would not be representative of the actual Plasmatron tests we want to perform if we cannot have a priori an accurate assessment of the catalytic response of quartz with respect to the TPS material.

For this reason, we devise two synthetic cases from different existing experimental data. On one hand, Panerai and Chazot [16] tested the TPS material we are interested in and obtained measurements of its surface temperature under conditions we can consider. On the other hand, Viladegut and Chazot [6] tested quartz and copper calorimeters together under similar conditions to Panerai and Chazot. The cases we are after concern the testing of quartz, copper and TPS under the same incoming flow conditions. Panerai and Chazot, and Viladegut and Chazot tested under the same static pressure which allows us to produce accurate linear regressions for $q_{\text{w}}^{\text{TPS}}$ and $T_{\text{w}}^{\text{TPS}}$ with increasing reference heat fluxes q_{w}^{Cu}. We use Viladegut and Chazot's measured reference heat fluxes to then retrieve the equivalent $q_{\text{w}}^{\text{TPS}}$

and T_w^{TPS} for Viladegut and Chazot's testing conditions. The actual data from Panerai and Chazot, and Viladegut and Chazot used to define our two synthetic cases as well as the different linear regressions can be found in Appendix A.

Table 1 shows the resulting synthetic cases. Two static pressures, 15 mbar and 50 mbar, are selected from the tests of Panerai and Chazot, and Viladegut and Chazot. One of the interesting aspects of this exercise is to see how sensitive the results are to different testing conditions, especially static pressures.

Table 1: Experimental data and uncertainties considered in our synthetic data study.

Experiment MTAs1	P_s [hPa]	q_w^{Cu} [kW/m^2]	T_w^{Cu} [K]	q_w^{Qz} [kW/m^2]	T_w^{Qz} [K]	P_d [Pa]	q_w^{TPS} [kW/m^2]	T_w^{TPS} [K]
Reported value	15	700	350	234	750	164	298	1561
Error std deviation (σ)	0.075	35	17.5	11.7	37.5	16.2	9.6	7.8
Experiment MTAs2	P_s [hPa]	q_w^{Cu} [kW/m^2]	T_w^{Cu} [K]	q_w^{Qz} [kW/m^2]	T_w^{Qz} [K]	P_d [Pa]	q_w^{TPS} [kW/m^2]	T_w^{TPS} [K]
Reported value	50	700	350	223	750	45	334	1600
Error std deviation (σ)	0.25	35	17.5	11.1	37.5	4.5	11.4	8

Fig. 3 shows the results for the two cases. The priors selected for these cases follow the same considerations as the case study of [14] given that we want to remain as agnostic as possible about the material behaviors in order not to introduce biasing issues. Thus, log-uniform distributions of range $\log \mathcal{U}[-4, 0]$ are used for all three materials in each case. In retrospective, more refined priors could be introduced for quartz for which its catalytic properties are better characterized in the literature, nevertheless we choose to stick to our previous analyses for consistency.

The marginal posterior distributions for the three catalytic parameters are what we were looking for with this experimental methodology. Copper and quartz lay well at the extremes of the catalytic parameter space, leaving the TPS marginal posteriors with significantly reduced supports and well-defined peaks. The accuracy of these results over del Val et al.'s case study clearly justifies the use of the proposed methodology. We continue forward and perform the real experiments.

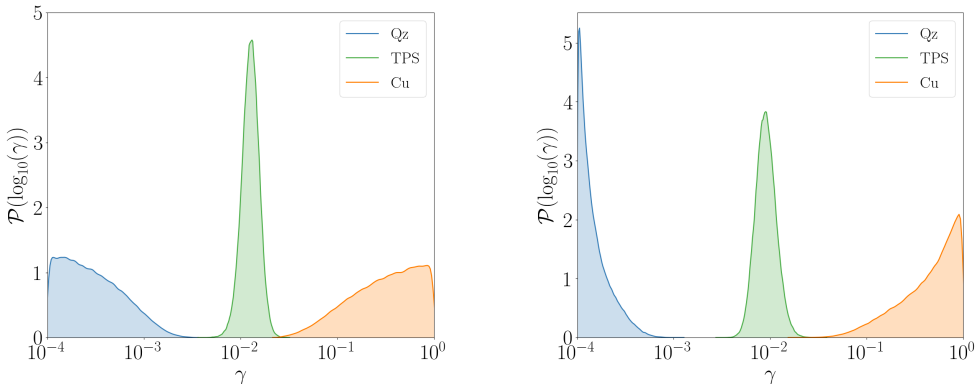

Figure 3: Marginal posterior distributions of the three catalytic parameters for MTAs1 (left) and MTAs2 (right).

4.2. Plasmatron testing conditions

The experimental test cases are chosen to study the impact of changing the heat flux for the same pressure (similar chemistry in the gas, higher TPS wall temperatures). Hence, heat fluxes of 500, 700 and 900 kW/m^2 are tested. Additionally, a higher static pressure (100 mbar) is tested for the same heat fluxes (where the gas is closer to chemical equilibrium). Thereafter, we compare the impact of changing heat fluxes and pressures in the posterior analysis. These cases are representative of material behaviors of copper and quartz, yielding good posterior distributions for the TPS

material. Therefore, we choose them for a first comprehensive study of the catalysis phenomena with the proposed set-up. A case with an intermediate static pressure of 50 mbar is also proposed as this case was used for reference in the works of Panerai and Chazot [16] and Viladegut and Chazot [6] for the comparison of the CMC material and quartz catalytic behaviors. An actual test and Bayesian analysis should settle the fact that quartz is indeed a lower catalytic material than CMC for those conditions.

To proceed with the experiments, the Plasmatron is switched on and the air mass flow is set with a calibrated rotameter. The vacuum pumps are then regulated until the target static pressure is reached inside the chamber. After that, the probe with the copper calorimeter is injected into the plasma and the power is regulated according to the target heat flux being measured, displayed and recorded in real time. Once the calorimeter reaches a steady-state signal under the imposed conditions, the probe is removed from the plasma jet and the one holding the quartz calorimeter is introduced. The heat flux is measured and the injection/ejection process is repeated for the TPS sample. Tables 2 and 3 summarize the experimental testing conditions and associated uncertainties based on the tests carried out with the set-up depicted in Sec. 2.2.

Table 2: Plasmatron testing conditions (15, 50 and 100 hPa, atmospheric air) for $\dot{m}$ = 16 g/s: targetted cold wall heat flux $q_w^{Cu,ref}$, dynamic pressure P_d, mean wall heat fluxes q_w^i and mean surface temperature T_w^{TPS}.

Test case	Coil power (W)	P_s (mbar)	$q_w^{Cu,ref}$ (kW/m^2)	P_d (Pa)	q_w^{Cu} (kW/m^2)	q_w^{Qz} (kW/m^2)	q_w^{TPS} (kW/m^2)	T_w^{TPS} (K)
MTAt1	157	15	500	121.48	493.57	219.35	227.79	1462.9
MTAt2	202	15	700	160.31	702.76	317.90	346.48	1631.0
MTAt3	281	15	900	196.6	898.39	374.13	417.23	1698.4
MTAt4	185	50	700	37.40	694.22	258.18	324.75	1585.6
MTAt5	177	100	500	13.60	492.56	251.00	302.49	1566.5
MTAt6	191	100	700	16.60	691.56	277.38	381.94	1655.8
MTAt7	205	100	900	19.62	892.48	337.04	470.45	1741.4

Table 3: Experimental uncertainties.

Test case	P_s (mbar)	$2\sigma_{P_s}$ (Pa)	$2\sigma_{P_d}$ (Pa)	$2\sigma_{q_w^{Cu}}$ (kW/m^2)	$2\sigma_{q_w^{Qz}}$ (kW/m^2)	$2\sigma_{q_w^{TPS}}$ (kW/m^2)	$2\sigma_{T_w^{TPS}}$ (K)
MTAt1	15	0.15	2.31	43.87	19.43	21.37	21.94
MTAt2	15	0.15	2.52	62.60	28.43	32.55	24.46
MTAt3	15	0.15	2.39	79.76	33.29	39.14	25.47
MTAt4	50	0.50	2.64	61.19	22.86	30.50	23.78
MTAt5	100	1.00	2.50	43.54	22.20	28.37	23.49
MTAt6	100	1.00	2.54	61.02	24.58	35.83	24.83
MTAt7	100	1.00	2.58	79.10	29.90	44.13	26.12

The uncertainty levels derived for this work in Table 3 are obtained following the same procedures as Viladegut [20], Panerai [5] and Helber [19], adopting the typical error values for the different measurements.

4.3. Results based on the experimental data

The main outcomes of the analyses are the γ_{TPS} marginal posterior distributions for the different test cases. In the next sections, the cases are divided according to the static pressure of the tests given that similar pressures produce comparable trends in the results.

4.3.1. 15 mbar cases

The γ_{TPS} marginal posterior distributions for MTAt2-3 present similar morphologies with bimodal distributions and values centered around $\gamma_{TPS} \approx 10^{-2}$ (Fig. 4). The results for MTAt1 are different in that the distribution for

γ_{TPS} presents a single peak, although the support is similar to MTAt2-3 and the distribution is also centered around $\gamma_{\mathrm{TPS}} \approx 10^{-2}$. The marginal posterior distributions for the auxiliary materials are also similar among them, favouring the extreme values of the catalytic parameter space. Even though the information of the relative catalytic efficiencies among materials is not given in the form of priors to the Bayesian analysis, the calibration ends up giving us this information from experimental data alone.

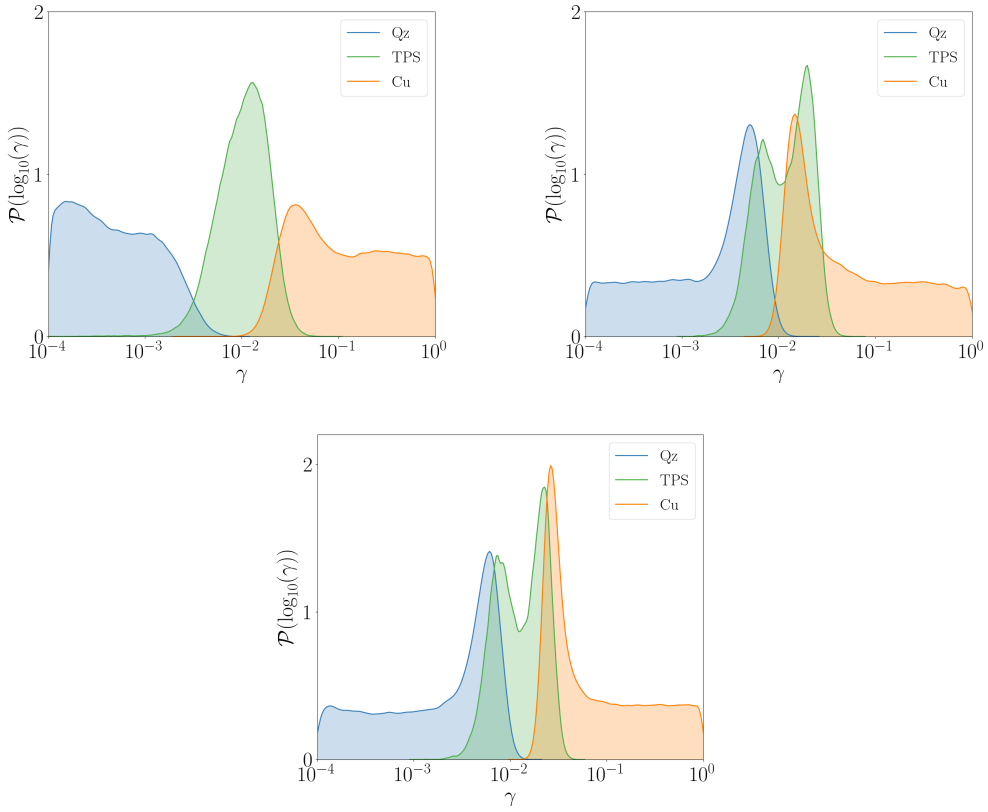

Figure 4: Marginal posterior distributions for the recombination parameters of the three materials at 15 mbar for MTAt1 (upper left), MTAt2 (upper right) and MTAt3 (lower center).

The results seem to indicate that the experimental set-up is useful for obtaining peaky distributions and reducing the uncertainty on the posterior of γ_{TPS} when compared to the previous work of del Val et al. [14]. Nevertheless, we still need to perform a careful assessment of the quality of the results. In particular, it is important to verify whether or not the calibration achieved can, in turn, predict the experimental data. It is not a trivial question, even for cases used for the calibration itself. Bayesian inference always gives some posterior distribution around the maximum likelihood estimate (in the case of non-informative priors, like the present study). It does not take into account the fact that the model might not be able to reproduce the experimental data for some combination of the parameters and the maximum estimate is just the best the model can do to reproduce the experimental data, but not enough. Through careful scrutiny, we can pinpoint successful cases and formulate new hypotheses for the cases that are not well calibrated, giving a way forward. Also this analysis can help gain more insight into the results.

The best way to visualize the quality of the inference is through the computation of the S-shaped curves. They represent the model output for the relationship between the boundary layer edge enthalpy H_δ and the catalytic efficiency parameter γ for given measurements $P_{\mathrm{s}}, P_{\mathrm{d}}, q_{\mathrm{w}}, T_{\mathrm{w}}$. In other words, they relate the possible values of the enthalpy H_δ and γ so that the prescribed measurements $P_{\mathrm{s}}, P_{\mathrm{d}}, q_{\mathrm{w}}, T_{\mathrm{w}}$ are predicted by the chosen model. Propagating the uncertainty of the measurements on these S-shaped functions gives us the boundaries of the allowed space where the curves should live if the model was a good description of the experiments. Comparing the prescribed boundaries

with the γ_{TPS} posterior and $H_{\delta}^{\mathrm{opt}}$ resulting distribution gives us an assessment of the quality of the inference and its deviation from the experimental data. Fig. 5 depicts the three S-shaped curves for each testing condition and the points drawn from the posterior distribution of $\gamma_{\mathrm{Cu}}, \gamma_{\mathrm{Ag}}$ and γ_{TPS}, and propagated to obtain $H_{\delta}^{\mathrm{opt}}$. As it can be seen, for the three cases considered under low pressure conditions, the calibrated $\gamma_{\mathrm{Cu}}, \gamma_{\mathrm{Ag}}$, and γ_{TPS} can successfully reproduce the experimental data.

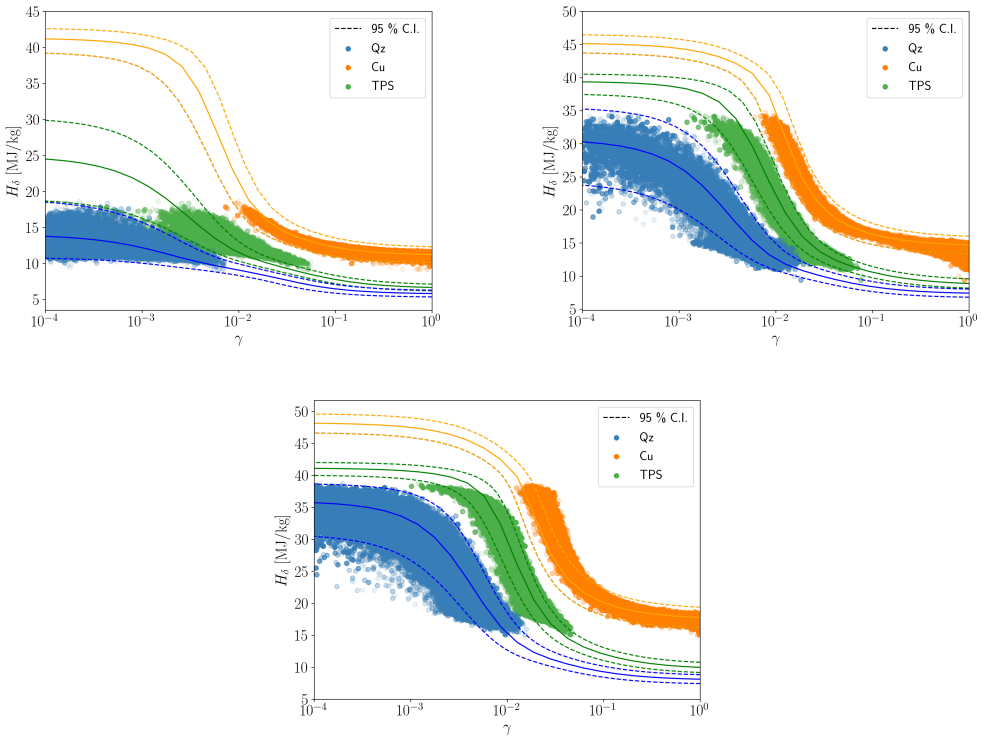

Figure 5: $\gamma_{\mathrm{Cu}}, \gamma_{\mathrm{Ag}}, \gamma_{\mathrm{TPS}}$ and $H_{\delta}^{\mathrm{opt}}$ distributions projected onto S-shaped curves and their 2σ confidence intervals for MTAt1 (upper left), MTAt2 (upper right) and MTAt3 (lower center).

4.3.2. 50-100 mbar cases

The γ_{TPS} marginal posterior distributions for these cases present similar morphologies with a well-defined peak and a reduced support compared to the previous low pressure cases (Fig. 6). Testing under higher pressures (50 and 100 mbar) give the most precise catalytic efficiencies, while relatively high heat fluxes and low pressure cases give more uncertain outcomes. In low pressure conditions, the chemistry does not play such an important role as in the higher pressure cases. The gas phase Damköhler number, defined as the ratio between the characteristic diffusion time and the chemical relaxation time $Da = \tau_{\mathrm{diff}}/\tau_{\mathrm{chem}}$, is small ($O(10^2)$) for low pressure cases. This indicates that we are in a reaction limited regime [58] and that the heat flux measured can be explained by widely different combinations of catalytic activity at the surface and edge conditions. Given fast diffusion time scales, catalytic activity at the surface becomes important as it modulates a considerable amount of diffusive flux. In these cases, convective and diffusive heat fluxes can be traded by modifying the recombination efficiencies, giving the same total heat flux measured. High pressure cases, on the other hand, tend to be in a diffusion limited regime (Damköhler number of the gas large, $O(10^6)$) and the modulation achieved by the recombination efficiency parameters is not so important, setting the diffusive flux to within certain values for which only a handful of edge conditions suffice to match the total heat flux measured. This reduction of the uncertainty that is case-dependent works better if the materials have very different catalytic behaviors.

Fig. 7 depicts the S-shaped curves for each testing condition. As it can be seen, for some of the cases considered under high pressure conditions, the calibrated $\gamma_{\mathrm{Cu}}, \gamma_{\mathrm{Qz}}, \gamma_{\mathrm{TPS}}$ cannot successfully reproduce the experimental data.

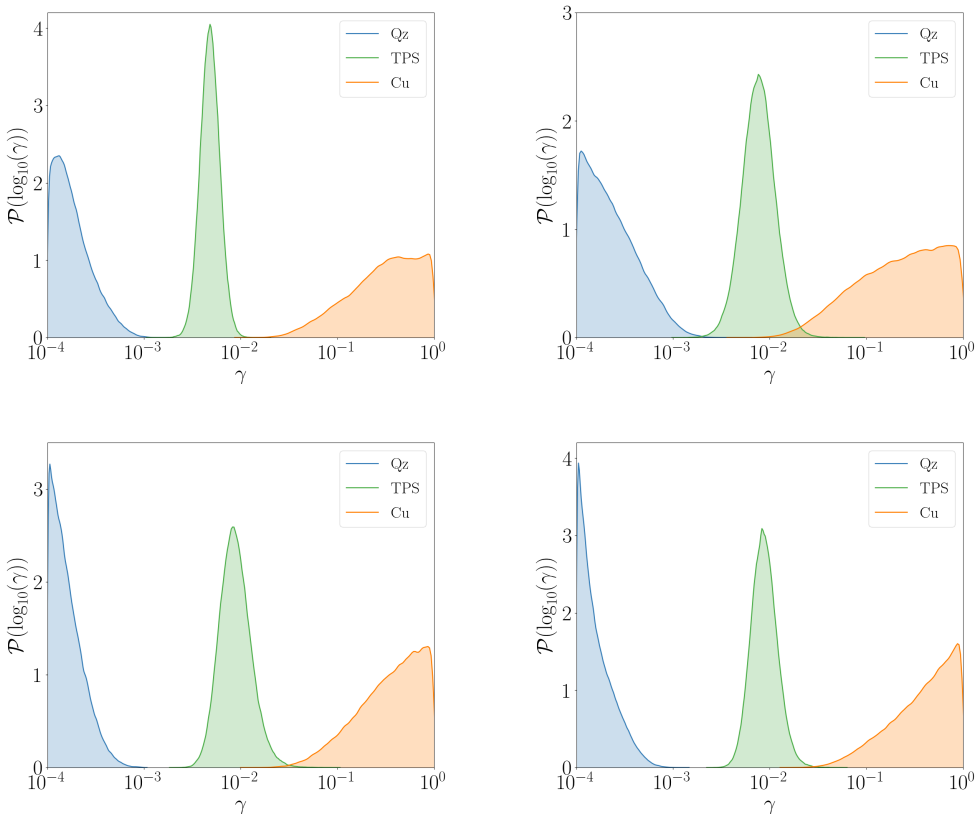

Figure 6: Marginal posterior distributions for the recombination parameters of the three materials at 50-100 mbar for MTAt4 (upper left), MTAt5 (upper right), MTAt6 (lower left) and MTAt7 (lower right).

Particularly, the posterior distributions of γ_{Qz}, γ_{Cu} and γ_{TPS} for cases MTAt6-7 cannot quite explain the experimental data measured in the Plasmatron. The resulting deviations are beyond the 3σ level of confidence. In other words, the model fails to simulate our experiments if there is not a single edge condition that can explain the different heat fluxes and surface temperatures observed. Looking at it in reverse, the model cannot predict all three heat fluxes under the requisite of a common edge condition. Therefore, in a follow-up analysis, we must highlight problematic assumptions beyond the ones considered here and properly assess our knowledge about them. There might be aspects of the system that are not known precisely in addition to the unknowns considered in this work (edge conditions and catalytic efficiency of all three materials).

4.4. Interpretation of results and summary statistics

In this section, we discuss the results obtained in Sec. 4.3 and draw a wider perspective about the problem in terms of modeling assumptions and future experimental data that might be of interest. The discussion is broken down according to the different static pressure of the experiments for the same reason as the presentation of the results in the previous section. Lastly, the summary statistics of the results are compiled in tables to compose a convenient experimental database for various uses.

15 mbar cases. It is seen that as the heat flux gets higher for the same pressure conditions, the sensitivity of the problem to γ is also higher (steeper S-shaped curves), broadening the span of possible solutions. Higher heat fluxes for the same pressure involves a higher degree of dissociation at the boundary layer edge as a consequence of the edge temperature increase. For a flow in a reaction limited regime (Damköhler number in the gas small), this higher

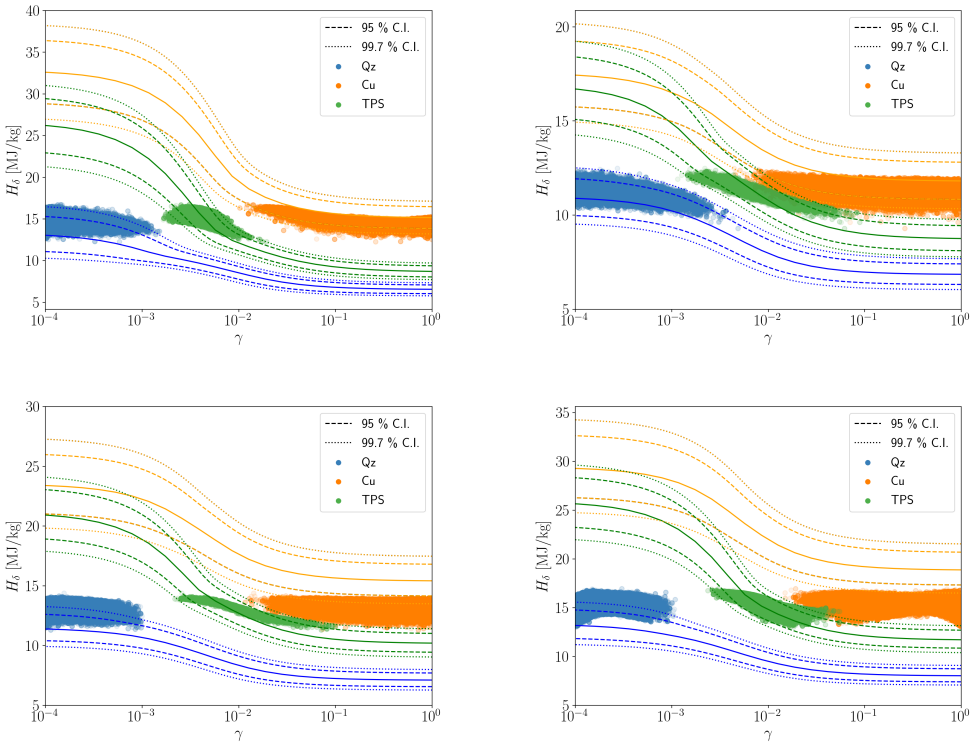

Figure 7: $\gamma_{Cu}, \gamma_{Ag}, \gamma_{TPS}$ and H_δ^{opt} distributions projected onto S-shaped curves and their 2σ and 3σ confidence intervals for MTAt4 (upper left), MTAt5 (upper right), MTAt6 (lower left) and MTAt7 (lower right).

dissociation degree means more sensitivity to surface reactions of the wall heat flux. Overall, higher heat fluxes produce wider supports for the reference materials (MTAt2-3) and two equally probable values of γ_{TPS} in the form of bimodal distributions. The lower γ_{TPS} peak corresponds to low values of γ_{Qz} and γ_{Cu}, while the opposite is observed for the upper γ_{TPS} peak. The obtained bimodal distributions for γ_{TPS} can be explained due to the fact that the priors assign the same probability to the different plausible values of the various decades of catalytic parameters. This issue, coupled with the high sensitivity of the problem to catalytic recombination at low pressures, produces two distinct favoured values in the posterior distributions. As can be seen in Fig. 5 most of the obtained posterior samples for MTAt2-t3 fall on one of the two plateaus of the optimal enthalpy with respect to the catalytic parameter γ. These two plateaus accummulate solutions for a certain range of catalytic parameters while favouring mainly two different values of the optimal edge enthalpy. Conversely, these two favoured values of the free stream also favour upper and lower limits on the γ_{TPS}. Both solutions are equally likely and more information is needed in either the priors or the experimental data to be able to pinpoint a more precise distribution.

From only looking at the marginal distributions it may seem that γ_{Qz} and γ_{TPS} both share simultaneous support for some values. As already mentioned, when γ_{TPS} values are taken from the lower peak (support shared with γ_{Qz}), the possible values for γ_{Qz} are the ones in the tail of the corresponding distribution. Due to the wall temperature differences, the model chosen can only consider low γ_{TPS} values for high boundary layer edge enthalpies. Conversely, for quartz, the γ_{Qz} values shared with γ_{TPS} can only be considered for substantially lower boundary layer edge enthalpies given the low wall temperature of the quartz probe. In other words, γ_{Qz} and γ_{TPS} cannot both have the same values simultaneously (which could be expected if an oxide layer of quartz forms on the TPS material surface). To actually gauge the importance of TPS oxidation on the determination of γ_{TPS} and how it actually compares to γ_{Qz}, longer tests to obtain a stable oxide layer and microscopic analyses of the structure could be pursued.

50-100 mbar cases. It is seen that for some of the cases considered under high pressure conditions, the calibrated $\gamma_{\mathrm{Cu}}, \gamma_{\mathrm{Qz}}, \gamma_{\mathrm{TPS}}$ cannot successfully reproduce the experimental data. Due to the complexity of the involved physics, we acknowledge that there might be aspects of the system that are not known precisely in addition to the unknowns considered in this work. One candidate for such unknown is the chemistry of the gas. The chemical state of the gas poses epistemic uncertainties given that different models exist in the literature and are widely used. Specifically, the speed of the different reactions considered can play a role in the inference, given that a flow in chemical equilibrium or frozen can produce very different heat fluxes under the same edge conditions. Catalytic activity can also be relegated to be non-influential in the heat flux experienced by the material if the gas chemistry has already consumed all the available energy contained in the dissociated flow, and this is likely to occur under high pressure conditions. A numerical experiment and a priori forward propagation of uncertainty can show if the effects of an uncertain gas chemistry would have an impact on the possible solutions for high pressure cases such as MTAt6 and MTAt7. The proposed exercise would indicate whether further analysis in that direction would be needed in the future. A numerical experiment is a good exercise to explore the models at hand while knowing exactly which assumption is not correctly considered in a synthetic reconstruction of simulated data. It is something not possible to achieve with experimental data due to the large number of unknowns involved, making difficult to have a definitive assessment of the effects some assumptions have. The following exercise highlights the impact of the adequacy of the gas phase chemistry model on the possible calibrated solutions. The results indicate that a model that overestimates the speed of chemical reactions in the flow can fail to reproduce the experimental data, while the opposite scenario would extend the uncertainty on the resulting calibrated parameters.

The numerical experiment is as follows. We simulate a boundary layer to which two different materials of high ($\gamma_{\mathrm{H}} = 1$) and low ($\gamma_{\mathrm{L}} = 10^{-4}$) catalytic efficiencies are subjected. The chosen conditions are similar to the experiments of this work and under the chemistry model of Gupta et al. [59]. This model considers the reactions to be slower than the alternative models of Park [60] and Dunn and Kang [38]. We choose the static pressure of such numerical experiment to be $P_{\mathrm{s}} = 100$ hPa, while the edge velocity is chosen so that we obtain a dynamic pressure $P_{\mathrm{d}} = 16.6$ Pa for an edge temperature of $T_{\delta} = 5500$ K, and Barker effect correction coefficient $K_{\mathrm{H}} = 1.1$ [47]. We impose the temperature at the wall for the high catalytic material to be $T_{\mathrm{w}}^{\mathrm{H}} = 350$ K while the low catalytic material has a wall temperature of $T_{\mathrm{w}}^{\mathrm{L}} = 750$ K similar to our copper and quartz probes. We also take the non-dimensional parameters (Sec. 3) to be the same as the case MTAt6 which would be equivalent to a Plasmatron power of 191 W and mass flow of 16 g/s. The uncertainties on all the considered measured quantities are consistent with the values reported in the literature for Plasmatron and in this work. The simulated heat fluxes are then taken as measurements from this numerical experiment with a $\pm 10\%$ uncertainty level for a 2σ confidence interval. We then compute the S-shaped curves from the simulated heat fluxes with their true chemistry in Fig. 8 (Gupta et al. model, continuous lines) and a faster chemistry model (Park, dashed lines). It can be appreciated that using a faster chemistry model when the heat fluxes correspond to a simulation with a slower gas chemistry model can result in S-shaped curves distancing away (or the opposite if the model used to reconstruct the simulated data uses a slower chemistry model than the original simulation). This issue can be evidence that in the high pressure experiments S-shaped curves do not overlap because the chosen model overestimates the speed of the chemical reactions in the gas phase.

Fig. 8 shows the line corresponding to the edge conditions of the numerical experiment which touches each S-shaped curve at the limits of their γ values as chosen for each material. In Fig. 8, it can also be seen that low catalytic efficiencies need lower enthalpies to produce the same heat flux with a faster chemistry model than with a slower one. Enthalpies for large catalytic efficiencies do not change under different gas chemistry models. This effect can be traced to the diffusive regime at the wall. The Damköhler number at the wall for large recombination efficiencies (fast wall chemistry) is large, meaning that we are in a diffusion limited regime. Different chemical models in the gas do not have an impact on the diffusive fluxes at the wall, setting the same outer edge conditions for all cases. On the other hand, reaction limited walls are more susceptible to the gas chemical models. Slower chemistry produces smaller concentration gradients which are easily overcome by species diffusion. This tendency produces smaller diffusion fluxes for the same pressure, which has to be compensated by larger temperature gradients across the boundary layer. As a result, higher enthalpies at the edge are required for the same heat flux in the case of slower chemistry at small wall Dankköhler numbers. It is equivalent to changing the Damköhler number of the flow to smaller values as the chemistry gets slower, while the diffusion time scale stays the same.

The right side of Fig. 8 shows the two S-shaped curves obtained with the Park chemistry model and their associated

confidence intervals when considering only the measurements as uncertain. In this scenario, an assumption of faster gas chemistry is considered where the actual data comes from a flow with slower chemistry. In this case, not even including the measurement uncertainties can give any solutions, or common edge conditions. The shaded grey area represents the added uncertainty when also the chemistry is assumed uncertain. The uncertainty on the chemistry is bounded by the slowest and fastest models that can be assumed for the problem, Gupta et al. and Park, respectively. This changes the picture by enabling possible solutions. Nonetheless, it can be observed that more than 50% of the resulting uncertainty for low catalytic values is due to the chemistry alone. The take away from this exercise is that the chemistry should be calibrated in dedicated experiments to obtain reliable predictions in the future, as it is shown to impact whether or not the chosen model can explain the experimental data, and this, in turn, influences the calibrated γ_{TPS} obtained. This issue was already studied by Viladegut et al. [58] from a different perspective. They studied different diffusion regimes while maintaining the same chemistry models and showed that the coupling between diffusion and chemistry in the flow has an impact on the computed values of catalytic efficiencies from experiments.

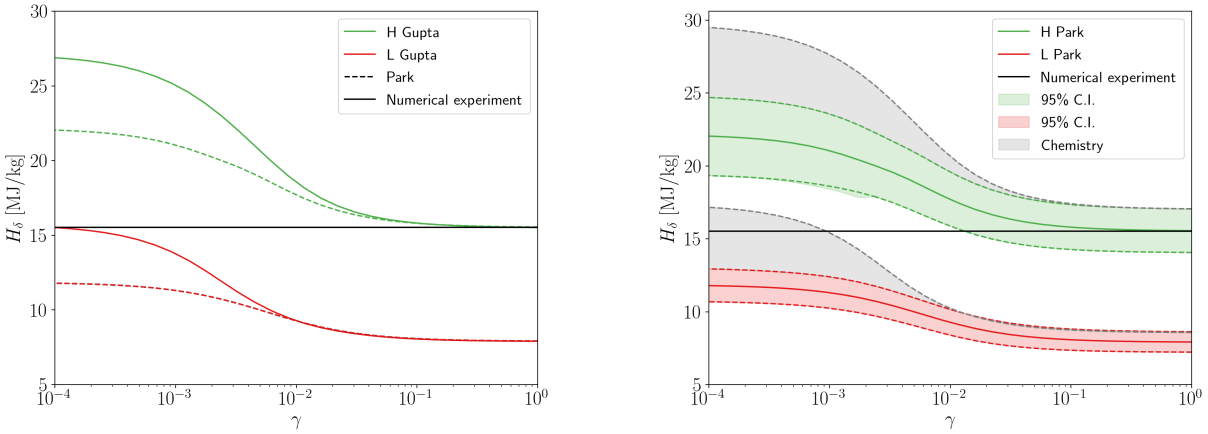

Figure 8: S-shaped curves for the chosen boundary layer simulation with slow and fast chemistry (left). Propagated uncertainty on the S-shaped curves of the numerical experiment, including uncertain chemistry models (right).

This issue does not influence the main outcomes of this study. If the adequacy of the chemical models are case-dependent, then for the same cases the proposed experimental methodology still should perform better under equal chemical model epistemic uncertainties. The major impact would be related to the final calibrated values and how those are affected by these epistemic uncertainties.

It is important to remark that the highlighted issues with the modeling of the gas phase chemistry are just one hypothesis given to explain the discrepancies observed in the results for high pressures. The likely real scenario might be a mix of different model inadequacies in various closures and assumptions, such as assumed elemental fractions at the boundary layer edge, thermal state of the gas, etc. The relevance of the numerical exercise rests on the capability to define new research avenues and identify further model issues.

Summary statistics. The resulting summary statistics for the different γ_{TPS} parameters are shown in Table 4. The resulting statistics for H_δ^{opt} after propagation of the calibrated parameters are shown in Table 5. Only the cases with successful inferences are shown.

5. Concluding remarks and outlook

In this work, we propose an experimental set-up for the precise calibration of uncertain catalytic efficiencies of CMC materials by using synthetic data and performing stochastic analyses. Further, plasma wind tunnel tests are

Table 4: γ_{TPS} marginal posterior distributions: mean, Maximum A Posteriori and 95% C. I. values.

Experiment ID	P_s [hPa]	Mean (μ) γ_{TPS}	MAP γ_{TPS}	95% C.I. γ_{TPS}
MTAt1	15	0.01	0.012	[0.0029, 0.0276]
MTAt2	15	0.011	0.019	[0.0036, 0.0289]
MTAt3	15	0.013	0.023	[0.0044, 0.0303]
MTAt4	50	0.0048	0.0048	[0.0030, 0.0076]
MTAt5	100	0.0077	0.0076	[0.0035, 0.0167]

Table 5: H_δ^{opt} distributions: mean, Maximum A Posteriori and 95% C. I. values.

Experiment ID	P_s [hPa]	Mean (μ) H_δ^{opt} [MJ/kg]	MAP H_δ^{opt} [MJ/kg]	95% C.I. H_δ^{opt} [MJ/kg]
MTAt1	15	12.6	11.5	[10.8, 15.7]
MTAt2	15	21.1	15	[14.3, 31.7]
MTAt3	15	26.0	17.8	[17.3, 36.7]
MTAt4	50	14.7	14.7	[13.9, 15.5]
MTAt5	100	11.2	11.2	[10.7, 11.7]

proposed and performed for which a compilation of summary statistics is computed, significantly enriching current catalytic recombination databases.

Our main contribution is the study of a experimental approach from a Bayesian perspective and the proposition of an experimental set-up and conditions that take into account the information content of the experiments. We start by assuming that not all knowledge about the system is known a priori (boundary layer edge conditions and catalytic efficiencies of the three materials) and that the measurements follow probability distributions based on the accuracy of the measurement devices. Given this, we explore the use of copper and quartz as auxiliary materials when tested along with the TPS material we want to characterize. This choice naturally brings more information to the model than testing with two probes as done previously. Also, the fact that the materials are quite different among them, in terms of catalytic activity promoted, increases the experimental information. The Bayesian formulation adopted to study this experimental set-up is the one developed by del Val et al. [14]. In that formulation, an optimal likelihood function is proposed to work with the experimental data involved in material characterizations for catalysis in the VKI Plasmatron. This formulation guarantees that we can learn the model parameters well enough to improve their characterization via experimental design as pursued in this work.

The proposed 3-probes testing methodology proves to be a good experimental approach due to the fact that the surface catalytic activity of the TPS material lays in between the catalytic activity of the two auxiliary materials chosen (copper and quartz). This conclusion is first reached by performing a synthetic case study which combines data from two different experimental campaigns available in the literature. The results of this synthetic study increase our confidence in the proposed methodology with which real experiments are performed in the VKI Plasmatron in the context of this study. A set of seven test cases is proposed under different static pressures and heat fluxes to study their influence on the results. The results show two different classes of characterizations achieved. First, for low pressures of 15 mbar, we show an improvement of 50 % over previous analyses of del Val et al. [14]. Even though it is still an improvement, we can appreciate a considerable support for the TPS material marginal distribution and a tendency towards following bimodal distributions.

In contrast, higher pressure cases such as 50 and 100 mbar, yield very precise parameters. Nevertheless, we should not lose sense of the fact that the gas chemistry is considered well-known. The diffusive fluxes in these cases are set in within some limits due to the chemistry being most likely in equilibrium, leaving little room for the outer edge enthalpy values which, in turn, are heavily conditioned. In this regard, a well characterized and precise TPS catalytic parameter can be obtained. The reduction of the uncertainty in this case is 30-50 % with respect to the previous 15 mbar cases and it relies solely on the chosen testing conditions. Nevertheless, not all the inferred parameters can be trusted. The model is found not to be a good representation of the experiments for two of the cases. Alternative

explanations such as the uncertainty on the chemical state of the gas could lead to an improvement.

In the future, dedicated experimental campaigns, including spectroscopic measurements, can benefit from this work by exploiting the experimental data more thoroughly and incorporating additional knowledge and uncertainties in terms of the gas phase chemistry.

Acknowledgements

The research of A. del Val was fully funded by the European Commission H2020 programme, through the UTOPIAE Marie Curie Innovative Training Network, H2020-MSCA-ITN-2016, Grant Agreement number 722734. Prof. Thierry Magin is acknowledged for his help and guidance. Andrea Fagnani, Alan Viladegut, Bernd Helber and Pascal Collin are acknowledged for their help and advice during the experimental campaign and post-processing of the measurements.

Appendix A. Extrapolation of Plasmatron testing conditions

The test case MTAs1 is based on Panerai and Chazot [16] and Viladegut and Chazot [6] experimental campaigns. The targeted reference heat flux for this analysis is 700 kW/m^2. However, as Panerai and Chazot did not target this heat flux, a scaling factor is applied. The actual testing conditions of Panerai and Chazot's work are summarized below in Table 6.

Table 6: Actual testing conditions extracted from Panerai and Chazot [16].

Test case	P_s [mbar]	q_w^{Cu} [kW/m^2]	P_d [Pa]	q_w^{TPS} [kW/m^2]	T_w^{TPS} [K]
k1a	15	410	127	174	1400
k1b	15	760	162	331	1600
k2a	15	1150	232	476	1800
k2b	15	1465	290	626	2000

Relations between the reference heat fluxes and each of the other parameters tested are found. The linear regressions, with respective R^2, obtained for each of the parameters are illustrated in Fig. 9 for the dynamic pressure, TPS heat flux and TPS wall temperature, respectively. The relations are summarized in Eqs. (9)-(11).

$$P_d = 0.1571 \times q_w^{Cu} + 54.08, \tag{9}$$

$$q_w^{TPS} = 0.4215 \times q_w^{Cu} + 2.89, \tag{10}$$

$$T_w^{TPS} = 0.5617 \times q_w^{Cu} + 1168.47. \tag{11}$$

The remaining testing conditions are extracted from Viladegut and Chazot's work as they tested quartz and copper together. The testing parameters are summarized in Table 7

Table 7: Actual testing conditions extracted from Viladegut and Chazot [6].

Test case	P_s [mbar]	q_w^{Cu} [kW/m^2]	q_w^{Qz} [kW/m^2]	Π_1 [-]	Π_2 [-]	Π_3 [-]	Π_4 [-]	Π_5 [-]
3a	15	700	233.8	0.4347	0.3137	0.5142	0.3407	0.4212

The scaling for any reference heat flux is done by replacing q_w^{Cu} in the previous equations by the targetted heat flux, in this case the 700 kW/m^2 from Viladegut and Chazot's experiment.

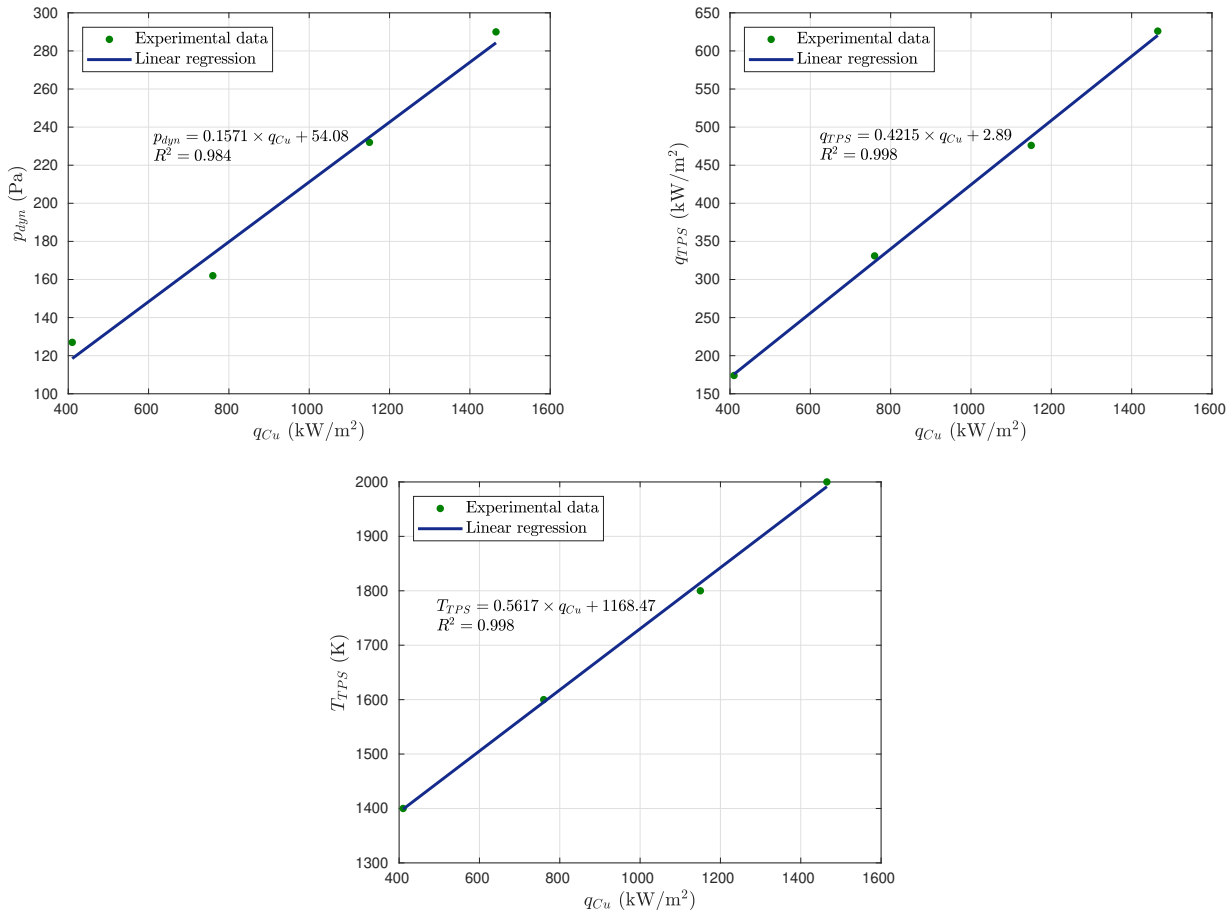

Figure 9: Linear regressions between dynamic pressure and copper heat flux (upper left), TPS and copper heat fluxes (upper right), and TPS wall temperature and copper heat flux (bottom center).

References

[1] O. Chazot, F. Panerai, High enthalpy facilities and plasma wind tunnels for aerothermodynamics ground testing in: Hypersonic Nonequilibrium Flows: Fundamentals and Recent Advances, Ed. Eswar Josyula ARLF, 2015.

[2] T. Magin, A model for inductive plasma wind tunnels, Ph.D. thesis, ULB/VKI (2004).

[3] B. Laub, E. Venkatapathy, Thermal protection system technology and facility needs for demanding future planetary missions, in: Proceedings of International Workshop on Planetary Probe Atmospheric Entry and Descent Trajectory Analysis and Science, 2004, pp. 239 – 247.

[4] R. Goulard, On catalytic recombination rates in hypersonic stagnation heat transfer (November 1958), Journal of Jet Propulsion 28 (11) (1958) 737–745.

[5] F. Panerai, Aerothermochemistry characterization of thermal protection systems, Ph.D. thesis, Università degli Studi di Perugia,von Karman Institute for Fluid Dynamics (2012).

[6] A. Viladegut, O. Chazot, Empirical Modeling of Copper Catalysis for Enthalpy Determination in Plasma Facilities (2019), Journal of Thermophysics and Heat Transfer 34.

[7] A. F. Kolesnikov, A. N. Gordeev, S. A. Vasil'evsky, Simulation of stagnation point heating and predicting surface catalycity for the EXPERT re-entry conditions., in: Sixth European Symposium on Aerothermodynamics for Space Vehicles, Moscow, Russia, 2008.

[8] S. Pidan, M. Auweter-Kurtz, G. Herdrich, M. Fertig., Recombination coefficients and spectral emissivity of silicon-carbide-based thermal protection materials (2005), Journal of Thermophysics and Heat Transfer 19 (4) (2005) 566–571.

[9] D. C. N. Sauvage, P. Tran, P. Vervisch, A. Bourdonand A. Desportes, EADS-LV and CORIA Common Approach on Catalycity Measurement, in: A. Wilson (Ed.), Hot Structures and Thermal Protection Systems for Space Vehicles, Vol. 521 of ESA Special Publication, 2003, p. 313.

[10] M. Schüßler, M. Auweter-Kurtz, G. Herdrich, S. Lein, Surface characterization of metallic and ceramic tps-materials for reusable space vehicles (2009), Acta Astronautica 65 (5) (2009) 676–686. doi:https://doi.org/10.1016/j.actaastro.2009.01.048.

[11] D. Stewart, T. Gokcen, S. Sepka, D. Leiser, M. Rezin, Development of a Catalytic Coating for a Shuttle Flight Experiment. doi:10.2514/6.2010-4321.

[12] A. del Val, Bayesian calibration and assessment of gas-surface interaction models and experiments in atmospheric entry plasmas, Ph.D. thesis, IPP/VKI (2021).
[13] K. Miki, M. Panesi, E. Prudencio, A. Maurente, S. H. Cheung, J. Jagodzinski, D. Goldstein, S. Prudhomme, K. Schulz, C. Simmons, J. Strand, P. Varghese, On the (In)Validation of a Thermochemical Model with EAST Shock Tube Radiation Measurements. doi:10.2514/6.2010-1557.
[14] A. del Val, O. P. Le Maître, T. E. Magin, O. Chazot, P. M. Congedo, A surrogate-based optimal likelihood function for the bayesian calibration of catalytic recombination in atmospheric entry protection materials (2021), Applied Mathematical Modelling (101) pp: 791-810.
[15] B. Bottin, O. Chazot, M. Carbonaro, V. Van Der Haegen, S. Paris, The VKI Plasmatron characteristics and performance (April 2000), Measurement Techniques for High Enthalpy and Plasma Flows.
[16] F. Panerai, O. Chazot, Characterization of gas/surface interactions for ceramic matrix composites in high enthalpy, low pressure air flow (2012), Materials Chemistry and Physics 134 (2-3) (2012) 597–607.
[17] B. Bottin, Aerothermodynamic model of an inductively-coupled plasma wind tunnel: Numerical and experimental determination of the facility performance, Ph.D. thesis, von Karman Institue for Fluid Dynamics (1999).
[18] T. M. Cheung, F. F. J. Schrijer, G. Park, Nitrogen Catalytic Recombination on Copper Oxide in Tertiary Gas Mixtures (2016), Journal of Spacecraft and Rockets 53 (2016) 644–653.
[19] B. Helber, Material response characterization of low-density ablators in atmospheric entry plasmas, Ph.D. thesis, von Karman Institute for Fluid Dynamics and Vrije Universiteit Brussel (January 2016).
[20] A. Viladegut, Assessment of gas-surface interaction modelling for lifting body re-entry flight design, Ph.D. thesis, VKI/UPC (2017).
[21] J. C. Greaves, J. W. Linnett, The recombination of oxygen atoms at surfaces, in: Trans. Faraday Soc., Vol. 54, 1958, pp. 1323–1330.
[22] J. C. Greaves, J. W. Linnett, Recombination of atoms at surfaces - part 5: Oxygen atoms at oxide surfaces, in: Trans. Faraday Soc., Vol. 55, 1959, pp. 1346–1354.
[23] R. A. Young, Measurements of the diffusion coefficient of atomic nitrogen in molecular nitrogen and the catalytic efficiency of silver and copper oxide surfaces (1961), The Journal of Chemical Physics 34 (1961) 1295.
[24] P. G. Dickens, Recombination of oxygen atoms on oxide surfaces. part 1.-activation energies of recombination, in: Trans. Faraday Soc., Vol. 60, 1964, pp. 1272–1285.
[25] R. A. Hartunian, W. P. Thompson, S. Safron, Measurements of catalytic efficiency of silver for oxygen atoms and the o-o2 diffusion coefficient (1965), The Journal of Chemical Physics 43 (1965) 4003.
[26] A. L. Myerson, Exposure-dependent surface recombination efficiencies of atomic oxygen (1969), The Journal of Chemical Physics 50 (1969) 1228.
[27] G. A. Melin, R. J. Madix, Energy accommodation during oxygen atom recombination on metal surfaces, in: Trans. Faraday Soc., Vol. 67, 1971, pp. 198–211.
[28] P. Cauquot, S. Cavadias, J. Amouroux, Thermal energy accomodation from oxygen atoms recombination on metallic surfaces (1998), Journal of Thermophysics and Heat Transfer 12 (2) (1998) 206–213.
[29] D. M. Driver, S. Sepka, Side arm reactor study of copper catalysis, in: 45th AIAA Thermophysics Conference, AIAA, 2015-2666.
[30] J. D. Anderson, Hypersonic and high-temperature gas dynamics, second ed., AIAA Education Series, 2006.
[31] P. F. Barbante, Accurate and efficient modelling of high temperature nonequilibrium air flows, Ph.D. thesis, ULB/VKI (2001).
[32] J. H. Ferziger, H. G. Kaper, Mathematical Theory of Transport Processes in Gases, North-Holland Publishing Company, 1972.
[33] M. Mitchner, C. H. Kruger, Partially Ionized Gases, John Wiley and Sons, Inc, 1973.
[34] S. Chapman, T. G. Cowling, The Mathematical theory of Non-Uniform Gases, Cambridge University Press, 1970.
[35] V. Giovangigli, Multicomponent Flow Modeling, Birkhauser, 1999.
[36] A. F. Kolesnikov, G. A. Tirsky, Hydrodynamics equations for partially ionised multicomponent gas mixtures with higher order approximations for transport coefficients, in: Fluid Mechanics-Soviet Research, Vol. 13 (4), 1984, pp. 70–97.
[37] K. K. Kuo, Principles of Combustion, John Wiley and Sons, Inc., 2005.
[38] M. Dunn, S. Kang, Theoretical and Experimental Studies of Reentry Plasmas, Tech. rep., NASA CR-2232 (1973).
[39] W. G. Vicenti, C. H. Kruger, Introduction to Physical Gas Dynamics, Krieger Pub Co., 1975.
[40] R. Goulard, On catalytic recombination rates in hypersonic stagnation heat transfer, in: Jet Propulsion, Vol. 28 (11), 1958, pp. 737–745.
[41] G. Degrez, D. V. Abeele, P. Barbante, B. Bottin, Numerical simulation of inductively coupled plasma flows under chemical non-equilibrium (2004), International Journal of Numerical Methods for Heat & Fluid Flow 14 (4) (2004) 538–558. doi:10.1108/09615530410532286.
URL https://doi.org/10.1108/09615530410532286
[42] D. V. Abeele, G. Degrez, Efficient Computational Model for Inductive Plasma Flows (2000), AIAA Journal 38 (2) (2000) 234–242. doi:10.2514/2.977.
[43] A. Lani, N. Villedieu, K. Bensassi, L. Koloszar, M. Vymazal, S. M. Yalim, M. Panesi, Coolfluid: an open computational platform for multi-physics simulation and research, in: 21st AIAA Computational Fluid Dynamics Conference, 2013-2589.
[44] G. Degrez, P. Barbante, M. de la Llave, T. E. Magin, O. Chazot, Determination of the catalytic properties of TPS materials in the VKI ICP facilities, in: European Congress on Computational Methods in Applied Sciences and Engineering ECCOMAS Computational Fluid Dynamics Conference 2001 Swansea, Wales, UK, 4-7 September 2001.
[45] J. B. Scoggins, V. Leroy, G. Bellas-Chatzigeorgis, B. Dias, T. E. Magin, Mutation++: Multicomponent thermodynamic and transport properties for ionized gases in c++ (2020), SoftwareX 12 (2020) 100575. doi:https://doi.org/10.1016/j.softx.2020.100575.
[46] I. Sakraker, Aerothermodynamics of Pre-Flight and In-Flight Testing Methodologies for Atmospheric Entry Probes, Ph.D. thesis, ULg/VKI (2016).
[47] M. Barker, On the use of very small pitot-tubes for measuring wind velocity (1922), Proceedings of the Royal Society A: Mathematical, Physical and Engineering Sciences 101.
[48] H. W. Krassilchikoff, Procedures for the determination of the cold copper catalycity, Tech. rep., VKI Project Report 2006-18, von Karman Institute for Fluid Dynamics (06 2006).
[49] F. Sanson, N. Villedieu, F. Panerai, O. Chazot, P. Congedo, T. E. Magin, Quantification of uncertainty on the catalytic property of reusable thermal protection materials from high enthalpy experiments (2016), Experimental Thermal and Fluid Science 82 (2016) 414–423.

[50] M. Kennedy, A. O'Hagan, Bayesian calibration of computer models (2001), Journal of the Royal Statistical Society: Series B 63 (2001) 425–464.
[51] N. Madras, Lectures on Monte Carlo Methods (Providence, 2001), American Mathematical Society.
[52] H. Haario, E. Saksman, J. Tamminen, An adaptive metropolis algorithm (2001), Bernoulli 7 (2001) 223–242.
[53] Y. M. Marzouk, H. N. Najm, Dimensionality reduction and polynomial chaos acceleration of bayesian inference in inverse problems (2009), Journal of Computational Physics.
[54] D. S. Sivia, J. Skilling, Data Analysis: A Bayesian tutorial, Oxford Science Publications, 2006.
[55] J. A. Nelder, R. Mead, A simplex method for function minimization (January 1965), Computer Journal 7 (4).
[56] D. Bursztyn, D. M. Steinberg, Comparison of designs for computer experiments (2006), Journal of Statistical Planning and Inference 136 (3) (2006) 1103 – 1119. doi:https://doi.org/10.1016/j.jspi.2004.08.007.
[57] M. D. McKay, R. J. Beckman, W. J. Conover, A comparison of three methods for selecting values of input variables in the analysis of output from a computer code (May 1979), Technometrics 21 (2) (1979) 239–245.
[58] A. Viladegut, U. Düzel, O. Chazot, Diffusion effects on the determination of surface catalysis in Inductively Coupled Plasma facility (2017), Chemical Physics 485-486 (2017) 88–97.
[59] R. Gupta, J. Yos, R. Thompson, K. Lee, A Review of Reaction Rates and Thermodynamic and Transport Properties for an 11-Species Air Model for Chemical and Thermal Nonequilibrium Calculations to 30000 K, Tech. rep., NASA RP-1232 (1990).
[60] C. Park, Nonequilibrium Hypersonic Aerothermodynamics, NASA Ames Research Center, Wiley, New York, 1989, pp. 255–268, 1989.